Available online at www.sciencedirect.com
ScienceDirect
International Journal of Multiphase Flow 32 (2006) 1370–1385
International Journal of Multiphase Flow
www.elsevier.com/locate/ijmulflow

Self-aeration and turbulence in a stepped channel: Influence of cavity surface roughness

M. Takahashi [a], C.A. Gonzalez [b,1], H. Chanson [c,*]

[a] Nihon University, College of Science and Technology, Department of Civil Engineering, 1-8 Kanda Surugadai, Chiyoda-ku, Tokyo 101-8308, Japan
[b] Cardno, Level 1, 5 Gardner Close, Milton QLD 4064, Australia
[c] Department of Civil Engineering, The University of Queensland, Brisbane, QLD 4072, Australia

Received 30 January 2006; received in revised form 4 July 2006

Abstract

The strong interactions between free-surface flows and atmospheric surroundings may lead to substantial air–water mixing with void fractions ranging from zero in clear-water to 100%. In this study, the air–water flow properties were studied in a large stepped water channel operating at large Reynolds numbers. Interactions between free-surface and cavity recirculation were systematically investigated in the skimming flow regime. Some surface roughness was introduced on the cavity walls and identical experiments were performed with several configurations. Basic results demonstrated some influence of step surface roughness on the flow properties leading to some counter-intuitive finding. The presence of cavity roughness was associated with higher flow velocities and comparatively lower turbulence levels. Distributions of bubble/droplet chords spanned over several orders of magnitude without significant influence of the cavity roughness. The distributions of turbulence levels and bubble count rates showed some correlation and highlighted strong interactions between entrained particles (bubbles, drops) and the flow turbulence.

Keywords: Air–water flows; Skimming flows; Cavity surface roughness; Bubbles; Droplets; Physical modelling

1. Introduction

Strong interactions between the flowing waters and the atmosphere may lead to substantial air–water mixing and complex multiphase flow situations (e.g. Chanson, 1997; Brocchini and Peregrine, 2001). Since the 1960s, numerous researchers studied gas entrainment in liquid flows focusing on low void fractions ($C < 0.05$) with relatively low Reynolds number flows. Few research projects have been engaged in strongly

* Corresponding author. Tel.: +61 7 33 65 35 16; fax: +61 7 33 65 45 99.
E-mail address: h.chanson@uq.edu.au (H. Chanson).
URL: http://www.uq.edu.au/~e2hchans/ (H. Chanson).
[1] Formerly at: Division of Civil Engineering, The University of Queensland, Brisbane, QLD 4072, Australia.

0301-9322/$ - see front matter © 2006 Elsevier Ltd. All rights reserved.
doi:10.1016/j.ijmultiphaseflow.2006.07.001

turbulent flows associated with free-surface aeration (Rao and Kobus, 1971; Wood, 1991; Chanson, 1997). One such flow situation is a high-velocity open channel flow skimming down steps (Fig. 1). This type of channel design is common in civil and environmental engineering structures (Ohtsu and Yasuda, 1998; Chanson, 2001). There may be some analogy between skimming flows over stepped chutes and skimming flows above large roughness elements, including boundary layer flows past d-type roughness. Chanson and Toombes (2002) presented new experimental evidence for the former. Djenidi et al. (1999) provided a comprehensive review of the latter configuration, while Aivazian (1996) studied zigzag strip roughness. Despite sometimes some conflicting interpretations, experimental results demonstrated interactions between the entrained air (self-aeration), the stream flow properties and the recirculation vortices that are observed below the pseudo-bottom formed by the step edges.

1.1. Dimensional analysis and similitude

The relevant parameters needed for a dimensional analysis include the fluid properties and physical constants, the channel geometry and inflow conditions, the air–water flow properties including the entrained air bubble characteristics, and the geometry of the steps. Let us consider a skimming flow down a stepped chute with flat horizontal steps in a prismatic rectangular channel. In the uniform equilibrium flow region, the gravity force component in the flow direction is counterbalanced exactly by the friction and drag force resultant. A complete dimensional analysis yields a relationship between the local air–water flow properties, and the fluid properties, physical constants, flow conditions and step geometry

$$C, \frac{V}{\sqrt{g*h}}, \frac{u'}{V}, \frac{d_{ab}}{h}, \ldots = \mathbf{F}_1\left(\frac{x}{h}; \frac{y}{h}; \frac{q_w}{\sqrt{g*h^3}}; \rho_w * \frac{q_w}{\mu_w}; \frac{g*\mu_w^4}{\rho_w*\sigma^3}; \frac{d}{h}; \frac{w}{h}; \theta; \frac{k_s'}{h}\right) \quad (1)$$

where C is the local void fraction, V is the local velocity, g is the gravity acceleration, h is the vertical step height (Fig. 2), u' is a characteristic turbulent velocity, d_{ab} is a characteristic size of entrained bubble, x is the coordinate in the flow direction measured from a step edge, y is the distance normal from the pseudo-bottom as shown in Fig. 2, q_w is the water discharge per unit width, ρ_w and μ_w are the water density and dynamic viscosity respectively, σ is the surface tension between air and water, W is the chute width, θ is the angle between the pseudo-bottom and the horizontal, k_s' is the equivalent sand roughness height of step surface and d is the equivalent clear-water depth defined as

Fig. 1. Photograph of rough stepped chute flow at Duralie coal mine stepped spillway NSW, Australia on 23 March 2005 (Courtesy of Tony MARSZALEK, Gilbert & Associates Pty LTD, Brisbane) – Slope: 1V:5H, $h = 0.5$ m, gabion construction.

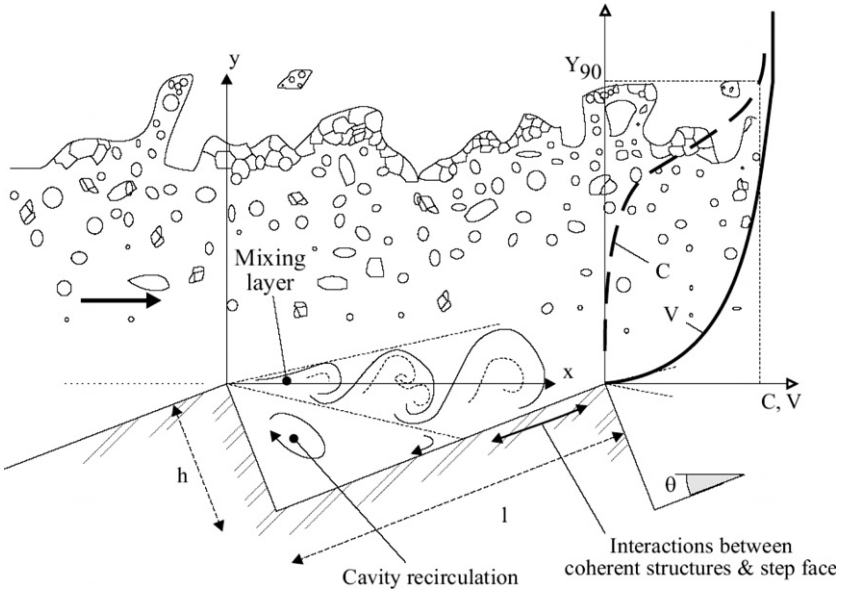

Fig. 2. Sketch of flow separation and developing mixing layer downstream of each edge on a stepped chute operating with skimming flow.

$$d = \int_{y=0}^{y=Y_{90}} (1 - C) * \mathrm{d}y \tag{2}$$

with Y_{90} being the depth where $C = 0.9$. In Eq. (1), the characteristic length scale is the vertical step height h. The right hand side terms include the dimensionless spatial coordinates x/h and y/h, and a Froude number, a Reynolds number and the Morton number, while the last four terms characterise the cavity shape and skin friction effect on the cavity wall.

In free-surface flows, most laboratory studies are based upon a Froude similitude since gravity effects are important (e.g. Henderson, 1966; Novak and Cabelka, 1981). This is also the case with stepped chute studies (e.g. Boes, 2000; Chanson and Gonzalez, 2005; Takahashi et al., 2005), but true dynamic similarity might not be achieved because of scale effects. Indeed cavity recirculation and momentum exchanges between cavity and

Table 1
Detailed experimental investigations of air–water flows in skimming flows on moderate slope stepped chutes

Reference	θ (degr)	q_w (m^2/s)	h (m)	$\frac{q_w}{\sqrt{g*h^3}}$	$\rho_w * \frac{q_w}{\mu_w}$	Remarks
(1)	(2)	(3)	(4)	(5)	(6)	(6)
Chanson and Toombes (2002)	21.8	0.06–0.18	0.10	0.61–1.82	6E+4–1.8E+5	$L = 3.0$ m. $W = 1$ m. Inflow: uncontrolled broad-crest. Nine steps
	15.9	0.07–0.19	0.10	0.79–1.54	7E+4–1.9E+5	$L = 4.2$ m. $W = 1$ m. Inflow: uncontrolled broad-crest. Nine steps
Gonzalez (2005)	21.8	0.075–0.22	0.10	0.76–2.22	7.4E+4–2.2E+5	$L = 3.3$ m. $W = 1$ m. Inflow: uncontrolled broad-crest. Ten steps
	15.9	0.020–0.20	0.05	0.2–2.02	2E+4–2E+5	$L = 4.2$ m. $W = 1$ m. Inflow: uncontrolled
		0.075–0.22	0.10	0.76–2.22	7.4E+4–2.2E+5	broad-crest. Nine steps
Present study	21.8	0.10–0.18	0.10	1.0–1.85	1E+5–1.8E+5	$L = 3.3$ m. $W = 1$ m. Inflow: uncontrolled broad-crest. Ten steps
Geometry 1						Smooth steps (painted marine ply)
Geometry 2a						Rough screens ($k_s' = 8$ mm) on both vertical and horizontal cavity faces
Geometry 2b						Rough screens ($k_s' = 8$ mm) on all horizontal cavity faces

Note: L: chute length.

stream flow are dominated by viscous effects while the entrapment of air bubbles and the mechanisms of air bubble breakup and coalescence are affected by surface tension effects. For geometrically similar models, it is impossible to satisfy simultaneously Froude, Reynolds and Morton similarities unless at full-scale. In small size models, the air entrainment process may be affected by significant scale effects discussed by Wood (1991) and Chanson (1997).

In the present study, a Froude similitude was used as for most open channel flow studies and past studies. The Morton number was also identical to civil and environmental engineering prototype applications since the fluids (air and water) were identical. The laboratory experiments were conducted in a large size facility operating at large Reynolds numbers (Table 1, column 6). These conditions are representative of full-scale storm waterways and could be considered as 3:1 to 6:1 scale studies of a stepped chute with step heights of 0.3–0.6 m.

Herein the writers investigate the interactions between entrained air and mainstream of skimming flows down an open channel. New experiments were conducted in a large stepped canal operating with Reynolds numbers between 1 and 1.8E+5. Interactions between free-surface and cavity recirculation were also investigated. The effects of cavity surface roughness were studied systematically with several configurations. The purpose of the present study was to investigate systematically the effects of step face roughness k_s'/h on skimming flow properties. The results provide new intriguing results on the effects of cavity roughness on the momentum exchange process.

2. Experimental setup

New experiments were conducted in a 3.3 m long, 1 m wide, 1V:2.5H slope chute ($\theta = 21.8°$) previously used by Chanson and Toombes (2002) and Gonzalez (2005). Waters were supplied from a large feeding basin (1.5 m deep, surface area 6.8 m × 4.8 m) leading to a sidewall convergent with a 4.8:1 contraction ratio. The test section consisted of a 1 m wide broad-crested weir with upstream rounded corner followed by 10 identical steps ($h = 0.1$ m, $l = 0.25$ m) made of marine ply. The stepped chute was 1 m wide with perspex sidewalls followed by a horizontal concrete-invert canal ending in a dissipation pit. Rough screens or triangular vanes could be installed on the steps (e.g. Chanson and Gonzalez, 2004; Gonzalez, 2005).

A pump supplied the waters and it was controlled with an adjustable frequency AC motor drive, enabling an accurate discharge adjustment in the closed-circuit system. Clear-water flow depths were measured with a point gauge. The discharge was measured from the upstream head above crest using a calibration curve derived from detailed velocity distribution measurements on the broad-crested weir (Gonzalez, 2005). Air–water flow properties were measured using a double-tip conductivity probe ($\varnothing = 0.025$ mm) designed at the University of Queensland. The probe sensors were aligned in the flow direction, the leading tip had a small frontal area (i.e. 0.05 mm^2) and the trailing tip was slightly offset to avoid wake disturbance from the first tip. An air bubble detector (UQ82.518) excited the probe and its output signal was scanned at 20 kHz per sensor for 20 s.

The translation of the probes in the direction normal to the channel invert was controlled by a fine adjustment travelling mechanism connected to a Mitutoyo^{TM} digimatic scale unit (Ref. No. 572-503).

Flow visualisations were conducted with high shutter speed digital still- and video-cameras. Further information on the experiments and the full-data sets were reported in Gonzalez et al. (2005).

2.1. Data processing, quality control, and data accuracy

The basic probe outputs were the void fraction, bubble count rate, air–water interface velocity, turbulence intensity estimate and air/water chord size distributions (e.g. Crowe et al., 1998; Chanson, 2002). The void fraction C is the proportion of time that the probe tip is in the air. The bubble count rate F is the number of bubbles impacting the probe tip per second. The air–water interface velocities were measured using a cross-correlation technique commonly used in large void fractions ($C > 0.10$). Turbulence levels were derived from the relative width of the cross-correlation function

$$Tu = 0.851 * \frac{\sqrt{\Delta T^2 - \Delta t^2}}{T} \quad (3)$$

where T is the air–water interfacial travel time for which the cross-correlation function is maximum, ΔT is the time scale for which the cross-correlation function is half of its maximum value such as: $R_{xy}(T+\Delta T) = 0.5 * R_{xy}(T)$, R_{xy} is the normalised cross-correlation function, and Δt is the characteristic time for which the normalised autocorrelation function equals: $R_{xx}(\Delta t) = 0.5$ (Chanson and Toombes, 2002). Physically, a thin narrow cross-correlation function ($\Delta T - \Delta t$ small) must correspond to little fluctuations in the interfacial velocity, hence a small turbulence level Tu. While Eq. (3) might not be equal to the turbulence intensity u'/V, it is an expression of some turbulence level or average velocity fluctuations. Chord sizes may be calculated from the raw probe signal outputs. The results provide a complete characterisation of the streamwise distribution of air and water chords although this analysis is restricted to the streamwise direction.

Phase-detection probes are sensitive devices and they are susceptible to a number of problems. In the present study, the quality control procedure developed by Toombes (2002, pp. 70–72) was applied thoroughly. Specifically, the probe signals were checked systematically for (1) long-term signal decays often induced by probe tip contamination, (2) short-term signal fluctuations caused by debris and water impurities, (3) electrical noise and (4) non-representative samples. While most quality control procedure can be automatised, it must be stressed that human supervision and intervention are essential to validate each quality control step.

The water discharge was measured with an accuracy of about 2%. The translation of the double-tip conductivity probe in the direction normal to the channel invert was controlled with an error of less than 0.5 mm. The accuracy on the longitudinal probe position was estimated as $\Delta x < \pm 0.5$ cm. The error on the transverse position of the probe was less than 1 mm. With the double-tip conductivity probe, the error on the air concentration (void fraction) measurements was estimated as: $\Delta C/C = 4\%$ for $0.05 < C > 0.95$, $\Delta C \sim 0.002/(1-C)$ for $C > 0.95$, and $\Delta C/C \sim 0.005/C$ for $C < 0.05$. The mean air–water velocities were computed with a cross-correlation technique. The analysis of the velocity field and chord length distributions implied no slip between the air and water phases. The error on the mean air–water interface velocity measurements was estimated as: $\Delta V/V = 5\%$ for $0.05 < C < 0.95$, $\Delta V/V = 10\%$ for $0.01 < C < 0.05$ and $0.95 < C < 0.99$ (Cummings and Chanson, 1997; Chanson and Brattberg, 1997). With the two-tip conductivity probe, the minimum detectable bubble chord length was about 150 μm in a 3 m/s flow based upon a data acquisition frequency of 20 kHz per channel.

2.2. Channel geometries and experimental flow conditions

Three types of cavity surface were tested (Table 1). The reference configuration (Geometry 1) consisted of smooth step faces. It was similar to the geometry used by Chanson and Toombes (2001, 2002) and Gonzalez (2005). Rough plastic screens with square patterns (16 mm size, 1 mm thick, 8 mm high) were used for the other two geometries. In Geometry 2a, the horizontal and vertical cavity faces were covered with the screen roughness (Fig. 3A). In Geometry 2b, only the horizontal step faces were covered with the rough screens (Fig. 3B).

The hydraulic roughness of plastic screens was tested in a 20 m long, 0.25 m wide tilting flume with glass sidewalls for a range of flow rates (0.017–0.04 m^3/s) and bed slopes (5–15%). The equivalent Darcy friction factor of the screens ranged from 0.05 to 0.08. Best fit with the Colebrook–White formula yielded an equivalent sand roughness height of 6.6 mm that was close to the plastic screen thickness $k'_s = 8$ mm.

Air–water flow measurements were conducted for flow rates ranging from 0.10 to 0.18 m^3/s corresponding to a skimming flow regime with Froude numbers $q_w/\sqrt{g * h^3}$ ranging from 1 to 1.85, and with Reynolds numbers $\rho_w * q_w/\mu_w$ between 1.0 and 1.8E+5 (Table 1). Measurements were performed systematically at step edges and at several locations between adjacent step edges above the recirculation cavities.

3. Basic air–water flow properties

3.1. Flow patterns

Waters cascading down stepped chutes are highly turbulent self-aerated flows. They are difficult to describe because of the different flow regimes observed. For a given chute geometry, the type of stepped flow regime is a function of the discharge. In the present study, skimming flow was observed for $q_w/\sqrt{g * h^3} > 1$ for all geometries.

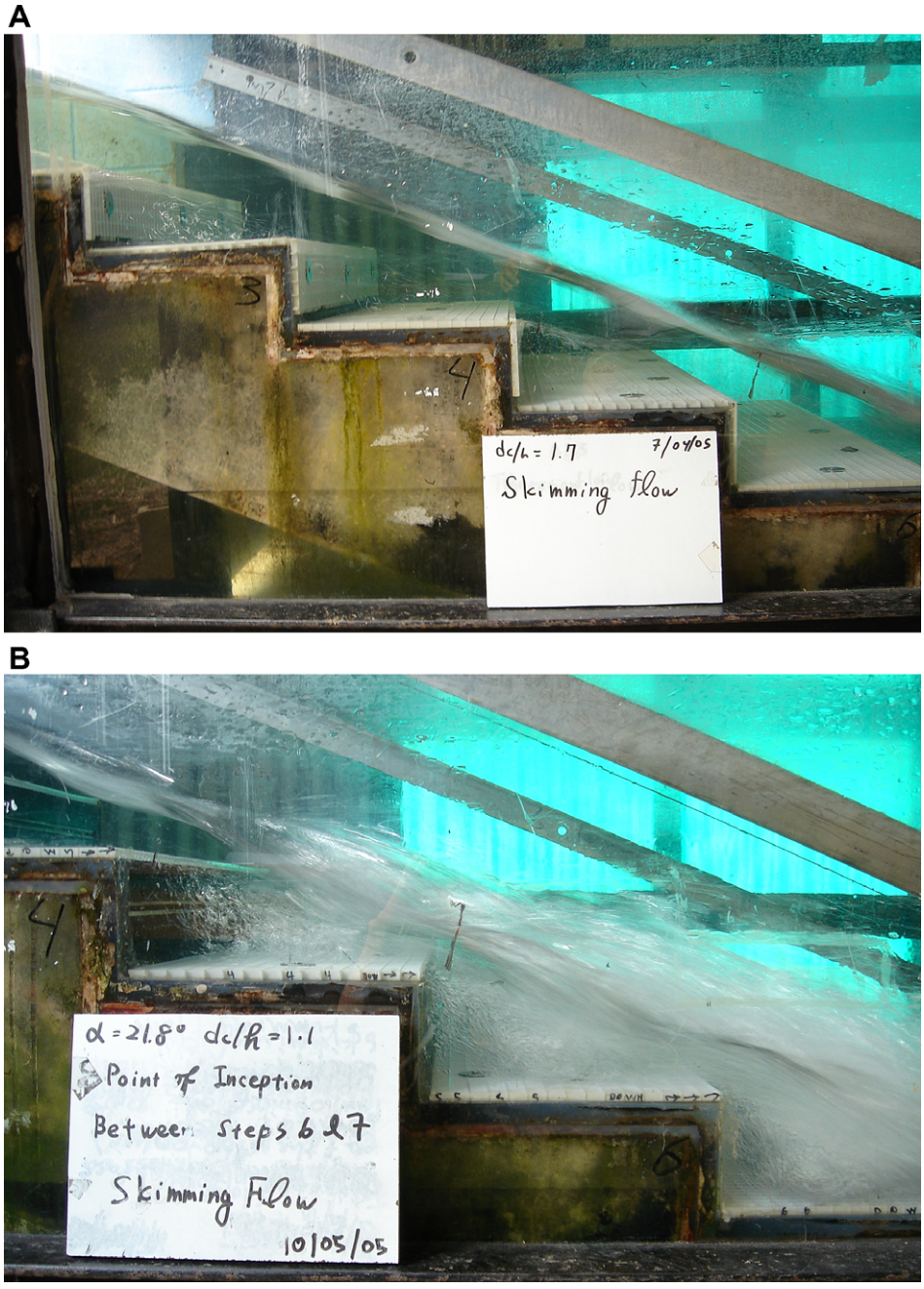

Fig. 3. Photographs of the experimental channel with rough cavities ($\theta = 22°$, $h = 0.1$ m). (A) Details of step roughness (Geometry 2a) in the clear-water flow region – $q_w/\sqrt{g * h^3} = 1.83$, $\rho_w * q_w/\mu_w = 1.8E+5$, $k'_s/h = 0.08$. (B) Skimming flow on rough steps (Geometry 2b) next to the self-aeration inception location – $q_w/\sqrt{g * h^3} = 1.15$, $\rho_w * q_w/\mu_w = 1.1E+5$.

In skimming flows, the water free-surface was smooth and no air entrainment occurred at the upstream end of the cascade (Fig. 3A). After a few steps the flow was characterised by a strong air entrainment (Fig. 3B). It is generally thought that the longitudinal position of inception of self-aeration corresponds to the position where the outer edge of the developing bottom boundary layer reached the free-surface (e.g. Halbronn, 1952; Wood et al., 1983). Downstream of the inception point, the two-phase flow behaved as a homogeneous mixture and the exact location of the interface became undetermined. There were continuous exchanges of air

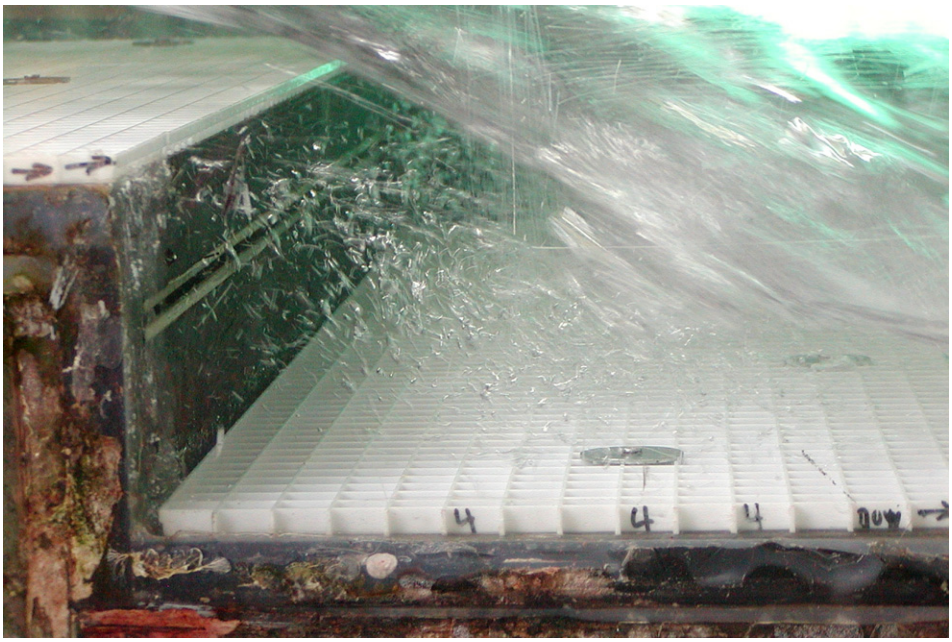

Fig. 4. Photograph of cavity aeration upstream of inception point of free-surface aeration ($\theta = 22°$, $h = 0.1$ m, Geometry 2b, $q_w/\sqrt{g * h^3} = 1.15$, $\rho_w * q_w/\mu_w = 1.1E+5$) – Details of air bubbles trapped in recirculating vortices in a cavity upstream of inception point of self-aeration.

and water, and of momentum, between main stream and atmosphere, while intense cavity recirculation was observed.

Next to the inception point of free-surface aeration, the flow was rapidly varied. Side view observations suggested that some air was entrapped by a flapping mechanism in the step cavity(ies) immediately upstream of the visual location of free-surface aeration. With smooth step faces, one to two cavities were typically aerated upstream the point of inception. In presence of cavity roughness, a greater number of aerated cavities was consistently seen upstream of the inception point, with typically three to four aerated cavities for Geometry 2a (rough vertical and horizontal faces) and two to three aerated cavities in Geometry 2b (rough

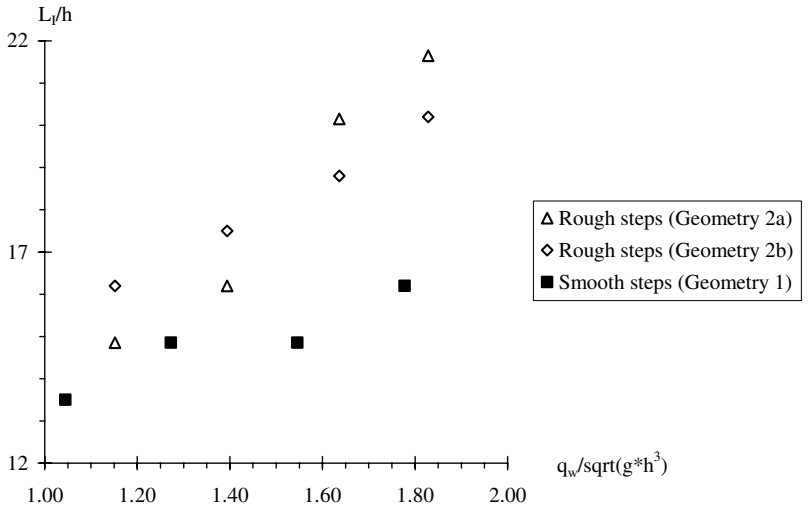

Fig. 5. Dimensionless location of inception point of free-surface aeration.

horizontal faces) (Fig. 4). Fig. 4 shows some air bubbles trapped in recirculation vortices upstream of the inception point of aeration.

The step roughness was seen to influence the location of the inception point of self-aeration. The inception point was located further downstream for chutes with rough cavity faces. This is illustrated in Fig. 5 which shows the dimensionless position of inception point as function of the Froude number $q_w/\sqrt{g*h^3}$, where L_I is the longitudinal distance between the downstream end of broad-crest and the inception point. With rough step cavities (Fig. 5, white symbols), free-surface aeration started about 30% further downstream than on the smooth step chute (Fig. 5, black symbols) for an identical flow rate. Present findings suggested a slower growth of the developing boundary layer on rough cavities associated with lesser rate of energy dissipation in the upstream clear-water flow region. This result is counter-intuitive compared to developing boundary layers

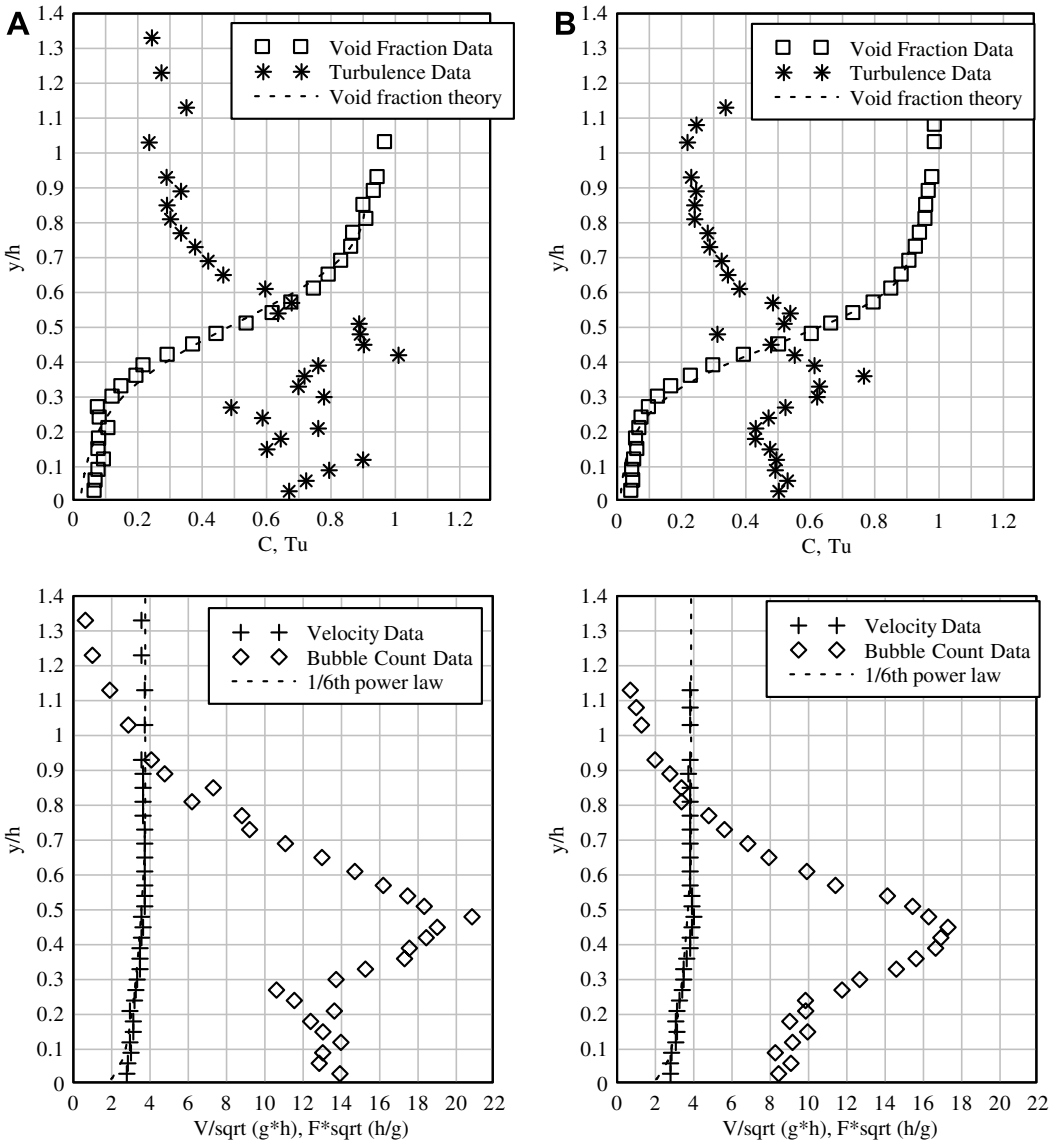

Fig. 6. Dimensionless distributions of void fractions, air–water interface velocities, turbulence levels and bubble count rate at a step edge, two cavity lengths downstream of inception point of self-aeration ($q_w/\sqrt{g*h^3} = 1.64$, $\rho_w * q_w/\mu_w = 1.6E+5$) – Left: Smooth steps (Geometry 1); Right: Rough steps (Geometry 2a).

and smooth-invert chute flows where increased bed roughness is associated with a shorter clear-water flow region (e.g. Wood et al., 1983).

3.2. Void fraction, turbulent intensity estimate and bubble count rate distributions

Downstream of the inception point of self-aeration, detailed measurements of void fraction, air–water interface velocity, turbulence levels and bubble count rates were conducted systematically at several longitudinal locations at step edges and between step edges. Fig. 6 illustrates some results obtained for the same flow rate at the same dimensionless location downstream of the inception point of self-aeration. Smooth step data are shown on the left (Fig. 6A and C) and rough step data are on the right (Fig. 6B and D).

For all step configurations, the void fraction distributions highlighted smooth profiles that were in close agreement with an analytical solution of the bubble advective diffusion equation in open channel flows. For $y > 0$, the data followed closely:

$$C = 1 - \tanh^2\left(K' - \frac{\frac{y}{Y_{90}}}{2D'} + \frac{\left(\frac{y}{Y_{90}} - \frac{1}{3}\right)^3}{3 * D'}\right) \quad (4)$$

where y is the distance normal to the pseudo-bottom (Fig. 2) formed by the step edge, Y_{90} is the characteristic distance where $C = 0.90$, K' and D' are integration constant functions of the mean void fraction only (Chanson and Toombes, 2002). Between step edges, strong aeration was also recorded. The results showed that cavity roughness induced slightly lesser self-aeration, especially in the recirculating cavities.

The air–water interface velocity distributions had a similar shape for all flow conditions and geometries. At each step edge, the velocity distributions had a shape that was close to a power law (as sketched in Fig. 2) for $C < 0.90$. In the upper flow region ($C > 0.90$), the values of the velocity were about constant, and the velocity profile was quasi-uniform. This is seen in Fig. 6C and D. However the velocity measurements showed some effect of cavity roughness that affected the cavity flow and extended into the main stream. The results showed consistently faster velocities on rough cavity chutes. Larger velocities and lower turbulence levels were observed systematically on rough step chutes at an identical dimensionless distance from the inception point of free-surface aeration. The findings were observed at both step edges and in-between the step edges suggesting that cavity roughness affected the entire flow field. Although the result might be counter-intuitive, the finding was observed systematically and it is illustrated in Fig. 6. Lower turbulence levels on rough step channels are seen in Fig. 6B compared to Fig. 6A, while larger air–water velocities are noted in Fig. 6D compared to Fig. 6C. It is thought that the cavity roughness affected flow separation at each sharp edge as well as shear layer development downstream of the singularity.

In terms of bubble count rates, the experimental data showed slightly smaller bubble count rates on rough step channel although the differences were small (e.g. Fig. 6C and D).

4. Air–water chord properties

Air–water flow records were analysed in terms of streamwise air bubble and water droplet chords. In regions of low void fraction ($C < 0.3$), air bubble chords were studied, while water droplet chords were analysed in spray regions defined as $C > 0.7$. In the intermediate zone ($0.3 < C < 0.7$), the air–water mixture is complex and it was difficult to identify the exact nature of the air–water flow because of the diversity in shape and size of the observed air–water structures. Toombes (2002) noted that the small probability of the probe tip piercing an air bubble or water droplet on its centreline further complicated the air–water structure identifying process.

Skimming flows comprise a broad range of chord sizes and it is common practice to present its distribution as a histogram (e.g. Chanson and Toombes, 2002; Toombes, 2002; Gonzalez, 2005). Typical results are shown in Figs. 7 and 8. For each figure, the caption and legend provide information on flow conditions, location y/h, local void fraction and number of recorded particles. The histogram columns represent each the probability of

bubble/drop chords in 0.5 mm intervals. For example, the probability of bubble chord from 1 to 1.5 mm is represented by the column labelled 1 mm. Bubble chord lengths larger than 20 mm are regrouped in the last column (>20). Fig. 7 presents data obtained at a step edge, and Fig. 8 shows data measured between step edges at $X = 0.25$ where X is the dimensionless longitudinal distance between two adjacent step edges with $X = 0$ and 1 at the cavity upstream and downstream ends respectively.

All the data showed the broad spectrum of bubble/drop chords at each location. The range of bubble/drop chord length extended over several orders of magnitude including at low void/liquid fractions from less than 0.1 mm to more than 20 mm. Further the distributions were skewed with a preponderance for small bubbles/droplets relative to the mean. In the bubbly flows ($C < 0.3$), bubble chord probability distribution functions followed closely a log-normal probability distribution function in all flow conditions and geometries. A similar finding was observed previously in skimming flows (e.g. Chanson and Toombes, 2002; Gonzalez, 2005).

The results in terms of number of detected bubbles/droplets and chord size distributions demonstrated that the structure of both bubbly and spray flows was similar for all the configurations above the pseudo-bottom. The finding implied that the cavity roughness did not affect significantly the microscopic-scale structure of the main flow ($y > 0$). However major differences were observed in the recirculation regions ($y < 0$). Smaller bubble chords were recorded on rough cavity configurations, because of a combination of lower void fractions in the cavity (highlighted by the existence of clear waters) and higher shear stresses induced by the cavity wall

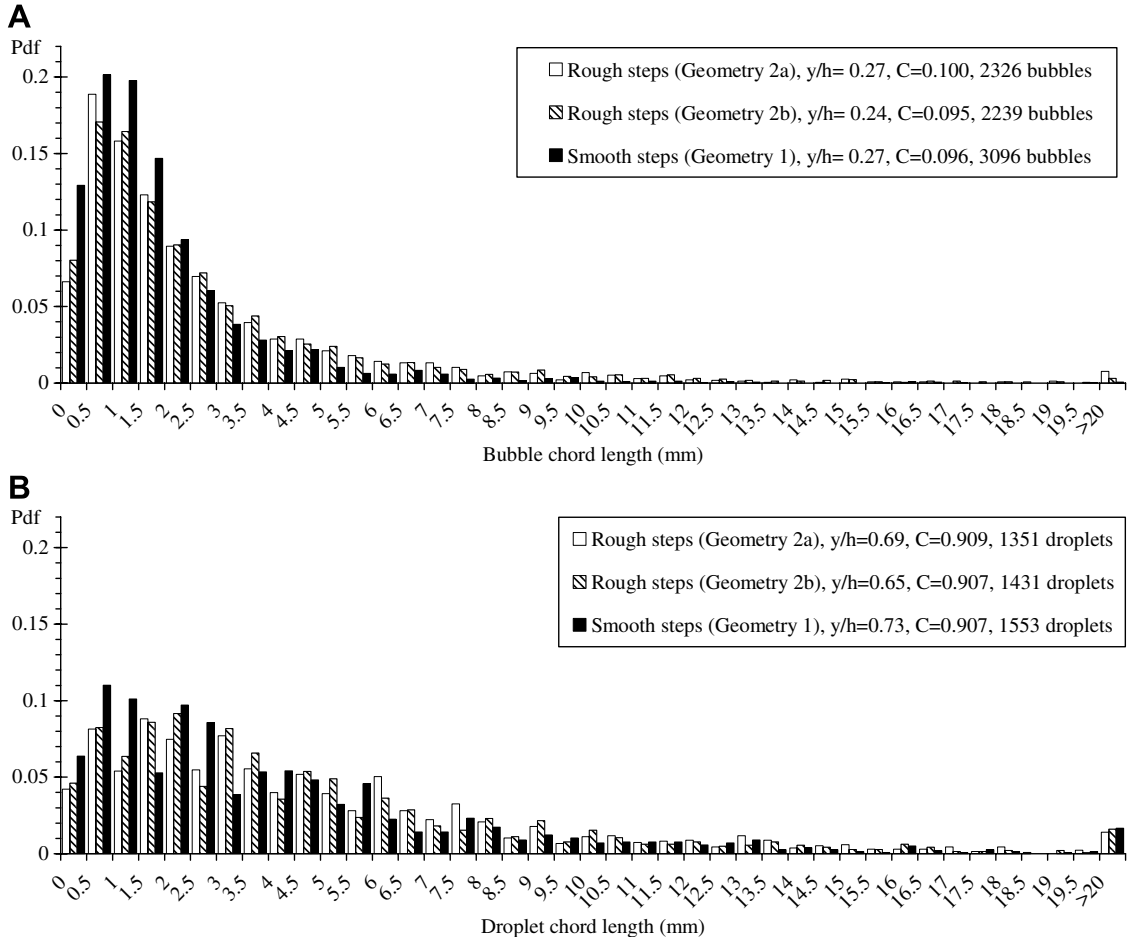

Fig. 7. Chord size distributions at step edge, two cavity lengths downstream of inception point of self-aeration ($\theta = 22°$, $h = 0.1$ m, $q_w/\sqrt{g * h^3} = 1.64$, $\rho_w * q_w/\mu_w = 1.6E+5$). (A) Bubble chord size distributions for $C = 0.1$. (B) Droplet chord size distributions for $C = 0.9$.

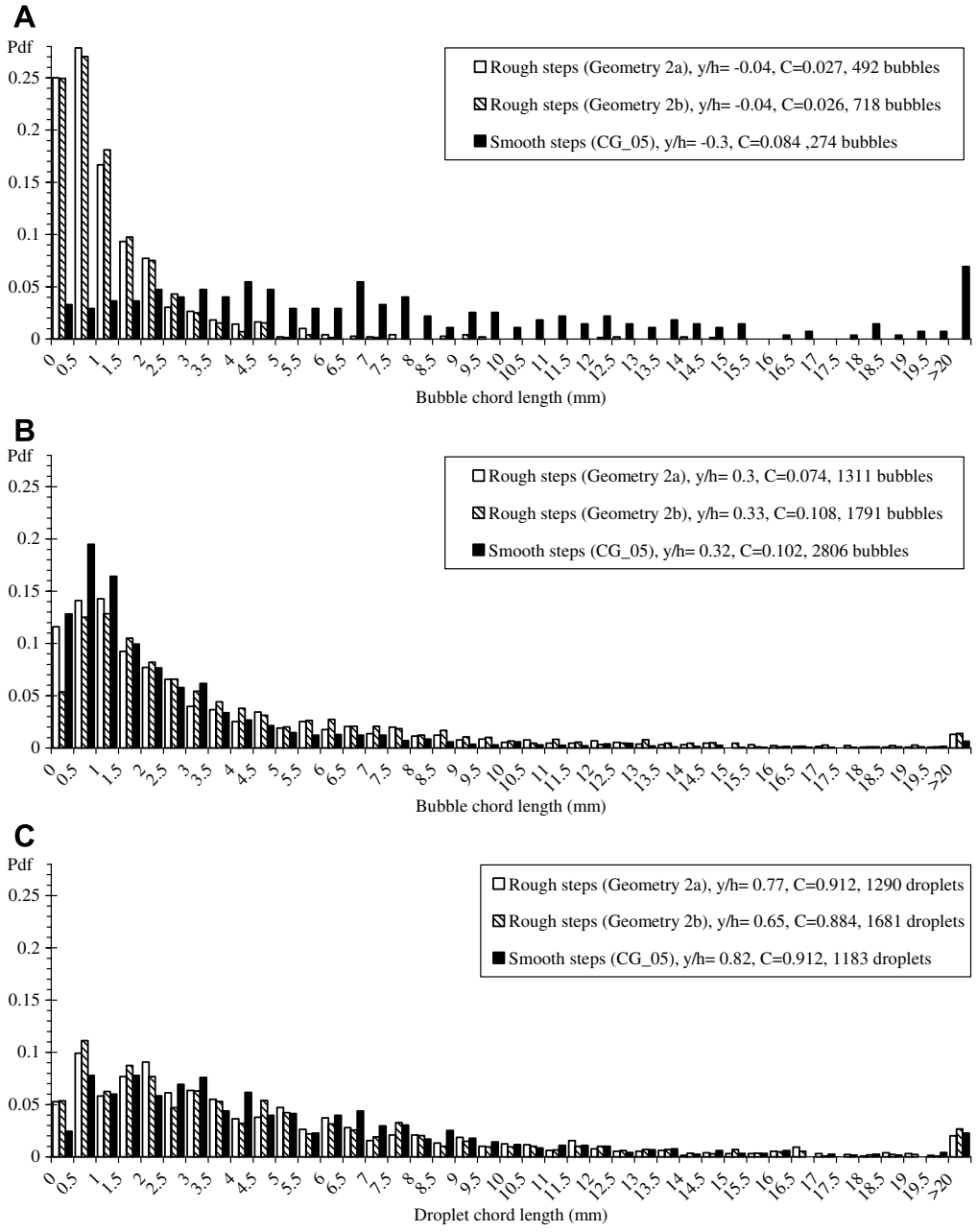

Fig. 8. Chord size distributions between step edges ($X = 0.25$) at 1.25 cavity lengths downstream of inception point of self-aeration ($\theta = 22°$, $h = 0.1$ m, $q_w/\sqrt{g * h^3} = 1.64$, $\rho_w * q_w/\mu_w = 1.6E+5$). (A) Bubble chord size distributions below the pseudo-bottom ($y < 0$). (B) Bubble chord size distributions for $C = 0.1$ above the pseudo-bottom ($y > 0$). (C) Droplet chord size distributions for $C = 0.9$ above the pseudo-bottom ($y > 0$).

roughness. Such a result is illustrated in Fig. 8A showing bubbly flow data recorded at an identical distance from the inception point of self-aeration for all tested geometries.

5. Discussion

In skimming flow on a stepped chute, the turbulence levels are markedly higher than turbulence intensities measured in monophase flows on a smooth invert (e.g. Ohtsu and Yasuda, 1997; Amador et al., 2004a). Ohtsu

and Yasuda (1997) and Amador et al. (2004a,b) measured turbulence intensities in skimming flows upstream of the inception point of self-aeration. With a 1-component LDA system, Ohtsu and Yasuda observed turbulence intensities u'/V of about 15–25%, while Amador and co-workers obtained turbulence intensities between 20% and 100% using a PIV system. Downstream of the inception point of air entrainment, experimental results showed enhanced turbulence levels for $0.1 < C < 0.9$ (Fig. 6A and B).

In the present study, all the data showed some correlation between turbulence levels Tu and bubble count rates associated with a monotonic increase in turbulence intensity with increasing bubble frequencies. This is illustrated in Fig. 9 which presents the relationship between turbulence level Tu and dimensionless bubble count rate $F * \sqrt{h/g}$ at several cross-sections. Present results were consistent with the earlier limited data sets of Chanson and Toombes (2002).

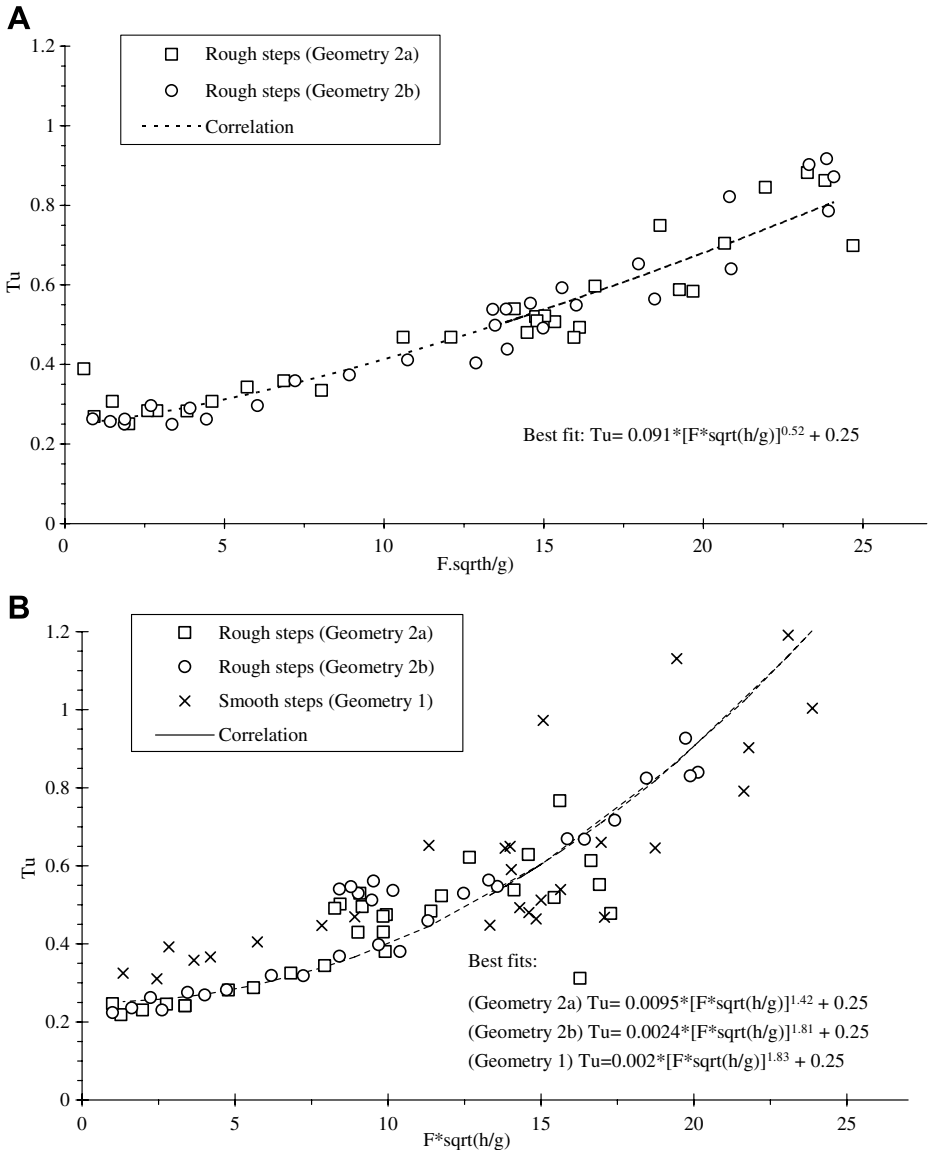

Fig. 9. Dimensionless relationship between turbulence levels and bubble count rates in skimming flow at the downstream end of the chute. (A) $q_w/\sqrt{g * h^3} = 1.39$, $\rho_w * q_w/\mu_w = 1.4E{+}5$, step edge 10, comparison with Eq. (5). (B) $q_w/\sqrt{g * h^3} = 1.64$, $\rho_w * q_w/\mu_w = 1.6E{+}5$, step edge 10, comparison with Eq. (5).

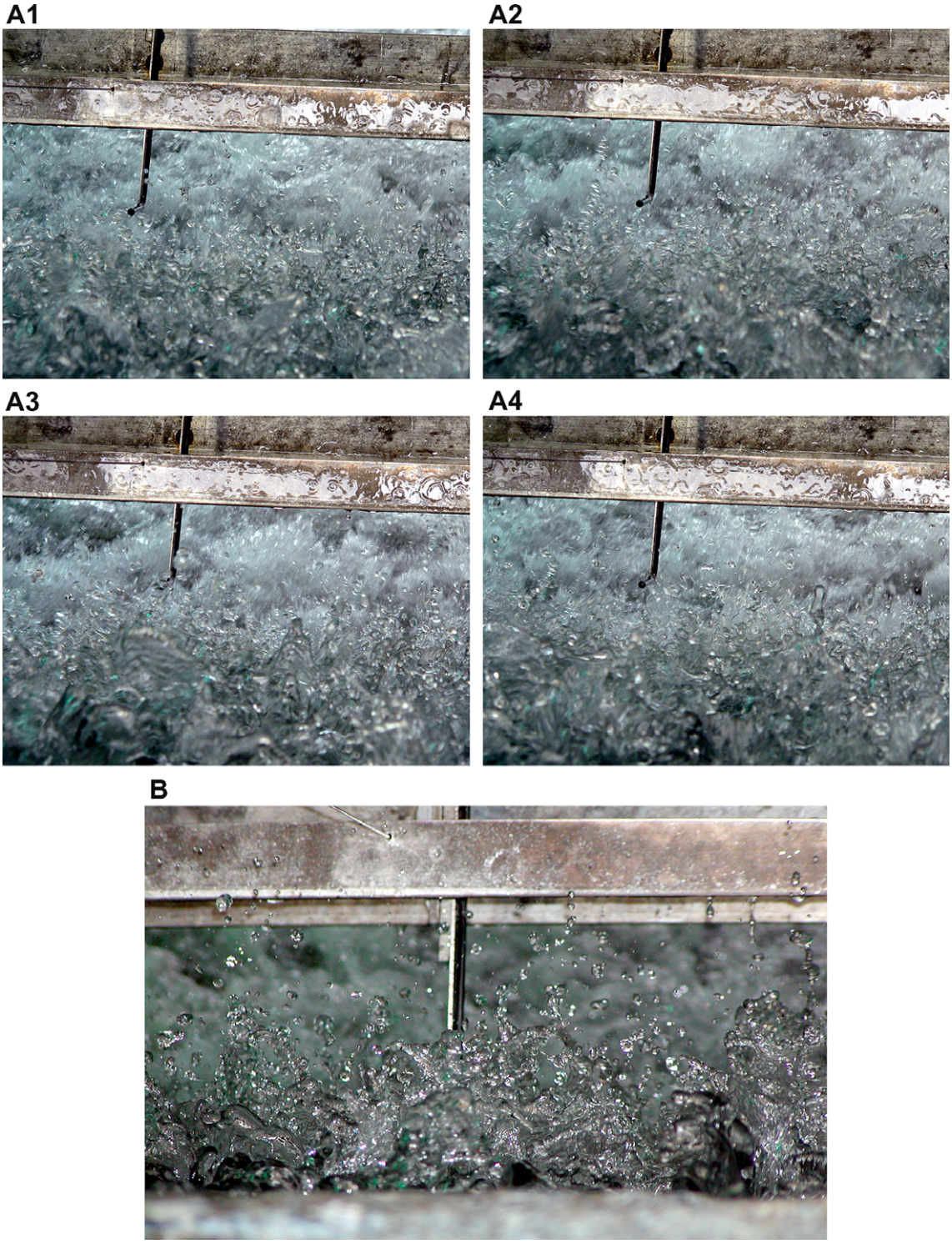

Fig. 10. Photographs of air–water exchanges in spray region looking downstream. (A) Spray above rough steps (Geometry 2a), $q_w\sqrt{g*h^3} = 1.39$, $\rho_w * q_w/\mu_w = 1.4E+5$, high-shutter speed (1/250 s) – sequence of four shots with 0.5 s between each photograph. (B) Rough steps (Geometry 2b), $q_w\sqrt{g*h^3} = 1.15$, $\rho_w * q_w/\mu_w = 1.1E+5$, inception point at step edge 6, probe located at step edge 8, high shutter speed (1/1000 s).

At step edges, the results suggested that:

$$Tu = 0.25 + \alpha * \left(F * \sqrt{\frac{h}{g}} \right)^{\beta} \quad (5)$$

where Tu is the turbulence level and F is the bubble count rate. For the present study, the coefficients α and β depended upon the discharge, step edge position and step configuration. β ranged from about 1.0 to 1.9 while α decreased with increasing distance from the inception point of free-surface aeration. The latter trend reflected a longitudinal monotonic increase in bubble count rate, while the levels of turbulence were roughly independent of the longitudinal location.

In skimming flow above a stepped invert, high-turbulence levels are generated by the step cavities. The resulting turbulent fluctuations acting next to the free-surface contribute to a drastic air entrapment and some advective dispersion. At the "pseudo-free-surface", air is continuously entrained and released (Fig. 10). The exact location of the "pseudo-free-surface" becomes undetermined, and very large bubble count rates were recorded (Figs. 6 and 9). The writers hypothesise that large bubble count rates, associated with large number of air–water interfaces, contribute to higher turbulence levels, compared to clear-water turbulent flows. This would be consistent with the strong correlation between turbulence levels and bubble count rates. For $0.05 \leqslant C \leqslant 0.95$, the air–water flow structure is dominated by collisions between particles (bubbles, droplets, packets) and by interactions between particles and turbulence. Such dynamic processes are associated with continuous bubble/droplet breakup, coalescence and interfacial deformations which contribute to large fluctuations in air–water interfacial velocity. Continuous modifications of air–water interfaces must induce large turbulence levels as measured by the intrusive phase-detection probe.

In the spray region, drop formation results from surface distortion, tip-streaming of ligaments and interactions between eddies and free-surface (e.g. Fig. 10). Once a droplet is ejected, its ejection process is the dominant effect because the droplet response time is nearly two orders of magnitude larger than the air flow response time. For void fractions between 0.70 and 0.99, measured droplet size distributions showed a broad range of droplet sizes from less than 0.05 mm up to more than 40 mm, with a mode around 2–5 mm. Above this spray layer, an upper spray field consisted primarily of very fine droplets (i.e. mist) with a few large (several millimetres) droplets reaching heights in excess of 10 equivalent clear-water depths (Fig. 10). Fig. 10A shows a sequence of four successive shots with 0.5 s between each photograph, illustrating the transient nature of the spray.

6. Conclusion

The interactions between free-surface, mainstream turbulent flow and cavity recirculation were studied in skimming flows down a stepped chute operating at large Reynolds numbers (Table 1). Two types of cavity surface were systematically investigated: smooth painted steps, and rough step cavities using 8 mm thick plastic screen elements.

The present results showed some similarities between all geometries. Similar flow patterns were typically observed, although the visual observations showed that the step cavity roughness affected the recirculation patterns. A major effect of the cavity roughness was the delay in the free-surface aeration inception. For the rough steps, the location of self-aeration inception was consistently displaced further downstream than on the smooth stepped chute for identical flow conditions. In turn, large air–water interface velocities were recorded on the rough cavity chutes. The finding contradicts the "intuitive" perception.

The local air–water flow measurements showed that larger velocities and lower turbulence levels were measured on the rough step chutes with identical flow conditions. The same trends were observed at step edges and between step singularities. The finding implied that the effects of cavity roughness extended throughout the entire flow field. The distributions of bubble and droplet chord sizes were recorded at each sampling location. The probability distributions functions of air/water chords were broad and spanned over two to three orders of magnitude. In the bubbly flow region ($C < 0.3$), the probability distribution functions of air chord sizes followed closely a log-normal law for all investigated configurations and flow conditions. The results in terms of probability distribution functions were close for all geometries. In the step cavities, smaller bubble

chords were measured in rough cavity configurations. Some correlation between turbulence levels and bubble count rates was observed for all flow conditions. It is believed that the finding highlights the existence of competing interactions between entrained bubbles and droplets, and the flow turbulence.

Overall the study provides new information on the complex interactions between turbulence and flow aeration in open channel flows at large Reynolds numbers. The results demonstrate further the "surprising" influence of step cavity roughness.

Acknowledgements

The writers thank Mr. G. Illidge for his technical assistance, and Professors I. Ohtsu and Y. Yasuda for their support. The study was undertaken while the first writer was a visiting scholar at the University of Queensland. The second writer acknowledges the financial support of the National Council for Science and Technology of Mexico (CONACYT) and of the University of Queensland.

References

Aivazian, O.M., 1996. New investigations and new method of hydraulic calculation of chutes with intensified roughness. Gidrotekhnicheskoe Stroitel'stvo, No. 6, pp. 27–39 (in Russian) (Translated in Hydrotechnical Construction, 1996, Plenum Publ., vol. 30, No. 6, pp. 335–356).

Amador, A., Sanchez-Juny, M., Dolz, J., Sanchez-Tembleque, F., Puertas, J., 2004a. Velocity and pressure measurements in skimming flow in stepped spillways. In: Yazdandoost, F., Attari, J. (Eds.), Proceedings of International Conference on Hydraulics of Dams and River Structures, Tehran, Iran. Balkema Publ., The Netherlands, pp. 279–285.

Amador, A., Van der graaf, G., Sanchez-Juny, M., Dolz, J., Sanchez-Tembleque, F., Puertas, J., 2004b. Characterization of the flow field in a stepped spillway by PIV. In: Proceedings of 12th Symposium on Applications Laser to Fluid Mechanics, Lisbon, Portugal, July 12–15, 10p.

Boes, R.M., 2000. Zweiphasenströmung und Energieumsetzung an Grosskaskaden. Ph.D. Thesis, VAW-ETH, Zürich, Switzerland.

Brocchini, M., Peregrine, D.H., 2001. The dynamics of strong turbulence at free surfaces. Part 1. Description. J. Fluid Mech. 449, 225–254.

Chanson, H., 1997. Air Bubble Entrainment in Free-Surface Turbulent Shear Flows. Academic Press, London, UK, 401p.

Chanson, H., 2001. The Hydraulics of Stepped Chutes and Spillways. Balkema, Lisse, The Netherlands, 418p.

Chanson, H., 2002. Air–water flow measurements with intrusive phase-detection probes. Can we improve their interpretation? J. Hyd. Eng. ASCE 128, 252–255.

Chanson, H., Brattberg, T., 1997. Experimental Investigations of Air Bubble Entrainment in Developing Shear Layers. Report CH48/97, Department of Civil Engineering, University of Queensland, Australia, October, 309p.

Chanson, H., Gonzalez, C.A., 2004. Interactions between free-surface, free-stream turbulence and cavity recirculation in open channel flows: measurements and turbulence manipulation. In: Matsumoto, Y., Hishida, K., Tomiyama, A., Mishima, K., Hosokawa, S. (Eds.), Proceedings of 5th International Conference on Multiphase Flow, Yokohama, Japan, Paper 104, 14p (CD-ROM).

Chanson, H., Gonzalez, C.A., 2005. Physical modelling and scale effects of air–water flows on stepped spillways. J. Zhejiang Univ. Sci. 6A, 243–250.

Chanson, H., Toombes, L., 2001. Experimental investigations of air entrainment in transition and skimming flows down a stepped chute. Application to Embankment Overflow Stepped Spillways. Research Report No. CE158, Department of Civil Engineering, The University of Queensland, Brisbane, Australia, July, 74p.

Chanson, H., Toombes, L., 2002. Air–water flows down stepped chutes: turbulence and flow structure observations. Int. J. Multiphase Flow 28 (11), 1737–1761.

Crowe, C., Sommerfield, M., Tsuji, Y., 1998. Multiphase Flows with Droplets and Particles. CRC Press, Boca Raton, USA, 471p.

Cummings, P.D., Chanson, H., 1997. Air entrainment in the developing flow region of plunging jets. Part 2: Experimental. J. Fluids Eng. Trans. ASME 119 (3), 603–608.

Djenidi, L., Elavarasan, R., Antonia, R.A., 1999. The turbulent boundary layer over transverse square cavities. J. Fluid Mech. 395, 271–294.

Gonzalez, C.A., 2005. An Experimental Study of Free-Surface Aeration on Embankment Stepped Chutes. Ph.D. Thesis, Department of Civil Engineering, The University of Queensland, Brisbane, Australia.

Gonzalez, C.A., Takahashi, M., Chanson, H., 2005. Effects of Step Roughness in Skimming Flows: an Experimental Study. Research Report No. CE160, Department of Civil Engineering, The University of Queensland, Brisbane, Australia, July, 149p.

Halbronn, G., 1952. Etude de la Mise en Régime des Ecoulements sur les Ouvrages à Forte Pente. Applications au problème de l'Entraînement d'Air. (Study of the Setting up of the Flow Regime on High Gradient Structures. Application to Air Entrainment Problem.) Jl La Houille Blanche, No. 1, pp. 21–40; No. 3, pp. 347–371; No. 5, pp. 702–722 (in French).

Henderson, F.M., 1966. Open Channel Flow. MacMillan Company, New York, USA.

Novak, P., Cabelka, J., 1981. Models in Hydraulic Engineering, Physical Principles and Design Applications. Pitman Publ., London, UK.

Ohtsu, I., Yasuda, Y., 1997. Characteristics of flow conditions on stepped channels. In: Proceedings of 27th IAHR Biennal Congress, San Francisco, USA, Theme D, pp. 583–588.

Ohtsu, I., Yasuda, Y., 1998. Hydraulic characteristics of stepped channel flows. In: Ohtsu, I., Yasuda, Y. (Eds.), Proceedings of Workshop on Flow Characteristics around Hydraulic Structures and River Environment, University Research Center, Nihon University, Tokyo, Japan, November, 55p.

Rao, N.S.L., Kobus, H.E., 1971. Characteristics of Self-Aerated Free-Surface Flows. Water and Waste Water/Current Research and Practice, 10. Eric Schmidt Verlag, Berlin, Germany.

Takahashi, M., Yasuda, Y., Ohtsu, I., 2005. Effect of Reynolds number on characteristics of skimming flows in stepped channels. In: Jun, B.H., Lee, S.I., Seo, I.W., Choi, G.W. (Eds.), Proceedings of 31st Biennial IAHR Congress, Seoul, Korea, pp. 2880–2889.

Toombes, L., 2002. Experimental Study of Air–Water Flow Properties on Low-Gradient Stepped Cascades. Ph.D. Thesis, Department of Civil Engineering, The University of Queensland.

Wood, I.R., 1991. Air entrainment in free-surface flows. IAHR Hydraulic Structures Design Manual No. 4, Hydraulic Design Considerations, Balkema Publ., Rotterdam, The Netherlands, 149p.

Wood, I.R., Ackers, P., Loveless, J., 1983. General method for critical point on spillways. J. Hyd. Eng. ASCE 109, 308–312.